AMERICAN SOCIETY FOR MICROBIOLOGY | Applied and Environmental Microbiology®

ENVIRONMENTAL MICROBIOLOGY

Deterioration-Associated Microbiome of Stone Monuments: Structure, Variation, and Assembly

Qiang Li,[a,b] Bingjian Zhang,[a,b] Xiaoru Yang,[c] Qinya Ge[d]

[a]Laboratory of Cultural Relics Conservation Materials, Department of Chemistry, Zhejiang University, Hangzhou, China

[b]Department of Cultural Heritage and Museology, Zhejiang University, Hangzhou, China

[c]Monitoring and Management Center of Hangzhou West Lake World Cultural Heritage, Hangzhou, Zhejiang, China

[d]Chinese Academy of Cultural Heritage, Beijing, China

ABSTRACT Research on the microbial communities that colonize stone monuments may provide a new understanding of stone biodeterioration and microbe-induced carbonate precipitation. This work investigated the seasonal variation of microbial communities in 2016 and 2017, as well as its effects on stone monuments. We determined the bacterial and fungal compositions of 12 samples from four well-separated geographic locations by using 16S rRNA and internal transcribed spacer gene amplicon sequencing. *Cyanobacteria* and Ascomycota were the predominant bacterial and fungal phyla, respectively, and differences in species abundance among our 12 samples and 2 years showed no consistent temporal or spatial trends. Alpha diversity, estimated by Shannon and Simpson indices, revealed that an increase or decrease in bacterial diversity corresponded to a decrease or increase in the fungal community from 2016 to 2017. Large-scale association analysis identified potential bacteria and fungi correlated with stone deterioration. Functional prediction revealed specific pathways and microbiota associated with stone deterioration. Moreover, a culture-dependent technique was used to identify microbial isolates involved in biodeterioration and carbonatogenesis; 64% of 85 bacterial isolates caused precipitation of carbonates in biomineralization assays. Imaging techniques including scanning electron microscopy with energy-dispersive spectroscopy, X-ray diffraction, and fluorescence imaging identified $CaCO_3$ crystals as calcite and vaterite. Although $CaCO_3$ precipitation induced by bacteria often has esthetically deleterious impacts on stone monuments, this process may potentially serve as a novel, environmentally friendly bacterial self-inoculation approach to the conservation of stone.

IMPORTANCE Comprehensive analyses of the microbiomes associated with the deterioration of stone monuments may contribute to the understanding of mechanisms of deterioration, as well as to the identification of potentially beneficial or undesirable microbial communities and their genomic pathways. In our study, we demonstrated that *Cyanobacteria* was the predominant bacterial phylum and exhibited an increase from 2016 to 2017, while *Proteobacteria* showed a decreasing trend. Apart from esthetic deterioration caused by cyanobacteria and fungi, white plaque, which is composed mainly of $CaCO_3$ and is probably induced by *Crossiella* and *Cyanobacteria*, was also considered to be another threat to stone monuments. We showed that there was no significant correlation between microbial population variation and geographic location. Specific functional genes and pathways were also enriched in particular bacterial species. The $CaCO_3$ precipitation induced by an indigenous community of carbonatogenic bacteria also provides a self-inoculation approach for the conservation of stone.

Received 1 December 2017 **Accepted** 25 January 2018

Accepted manuscript posted online 26 January 2018

Citation Li Q, Zhang B, Yang X, Ge Q. 2018. Deterioration-associated microbiome of stone monuments: structure, variation, and assembly. Appl Environ Microbiol 84:e02680-17. https://doi.org/10.1128/AEM.02680-17.

Editor Alfons J. M. Stams, Wageningen University

Address correspondence to Bingjian Zhang, zhangbiji@zju.edu.cn.

KEYWORDS stone monuments, microbiome, cyanobacteria, biomineralization, fluorescent imaging

Recently, considerable research has focused on the biodeterioration and biodegradation of stone works important to our cultural heritage, including ancient monuments, historic buildings, and artworks (1–5). Microorganisms, which include bacteria, fungi, algae, and lichens, colonize stone monuments exposed to outdoor environments and cause significant stone deterioration, as the regular stone matrix is reduced to a disordered internal structure. Among these microbial communities, cyanobacteria and algae, as phototrophs, may have greater ecological importance than any other organisms, as they are pioneer organisms that can initially settle on exposed stone monuments (6–9), which facilitates the colonization and growth of subsequent heterotrophic microflora. These autotrophs are resistant to extreme environmental stressors such as high temperatures, high levels of light intensity, and extreme desiccation (10–12). Cyanobacteria can synthesize and excrete extracellular polymeric substances (EPS), which are composed primarily of polysaccharides and protect against desiccation and intense solar radiation. However, EPS exposure causes stone decay and enhances biodeterioration (9, 13). Cyanobacteria can also solubilize calcium salts by producing chelating agents and corrosive acids and thereby trap released calcite particles to bind calcium ions around the cells (14). The detrimental effects of lichens and chemolithotrophic bacteria on stone monuments are esthetic damage and changes in the physicochemical properties of the monument structure. For example, lichens cause damage to stone matrices by means of hyphal penetration and secretion of acidic metabolites such as carbon dioxide, lichenic acids, and oxalic acid, while sulfur-oxidizing and nitrifying bacteria can convert inorganic sulfur and nitrogen compounds to sulfuric or nitrous acid. Finally, these acids dissolve calcareous rocks, leading to calcified encrustation formation and causing irreversible damage to outdoor stone monuments (3, 14, 15).

Bacterial carbonate precipitation is a natural phenomenon associated with different bacterial types, the most common of which are chemoorganotrophic bacteria (16, 17). Two hundred ten bacterial strains, including *Pseudomonas* and *Bacillus* strains, isolated from soil have been observed to form calcium carbonate crystals (18). Calcium carbonate biomineralization is a common result of bacterial colonization but is rarely caused by eukaryotic species (19–21). Two biomineralization mechanisms have been identified: biologically controlled and biologically induced mineralization (22). Calcium carbonate precipitation by bacteria is considered to be a biologically induced form of mineralization (16, 23–25). Bacterial calcification processes are strongly dependent on environmental conditions, metabolic activities, and cell surface structures. In general, the acidic metabolites secreted by bacteria and inorganic acids in the environment can dissolve calcium into positively charged Ca^{2+} ions; under neutral pH conditions, these ions can bond to negatively charged EPS fluids or to proteins present on cell surfaces. The interactions between bacterial surfaces and Ca^{2+} ions may change the initial charge distribution and aggregate bacteria into a heterogeneous nucleation (14, 16, 17, 26–28). According to previous studies, calcium carbonate precipitation should occur on the surface of the biofilm; however, recent studies using techniques for real-time *in situ* imaging of calcium precipitation processes have found that biomineralization began at the base (4). Although biomineralization induced by microorganisms may lead to evident esthetic changes in stone monuments, it may also serve as a consolidation technique to restore cultural relics (29).

In this study, we sequenced the epilithic microbiota from 12 samples that were collected in 2016 and 2017 at four well-separated geographic locations in China. We checked whether microbial communities from samples from different archaeological sites or from different times were taxonomically or functionally distinct. We performed systematic association analysis and identified specific bacterial and fungal taxa correlated with stone deterioration. Additionally, culturable bacterial and fungal strains were

recovered from stone blocks. Because of their detrimental effect on stone, bacterial isolates were used to determine carbonatogenic capacity, however, calcium carbonate precipitation induced by carbonatogenic bacteria can be used as a novel and environmentally friendly approach to consolidate stone.

RESULTS

Analysis of microbial colonization. Historical monuments, which are composed mainly of limestone and marble, show different visual defects due to different microbial colonizers. Samples with signs of biodeterioration and scanning electron microscopic (SEM) imaging of test specimens revealed striking differences among samples collected at four archaeological sites (Fig. 1). When classified by colony morphology and colonization appearance, a total of five detailed categories involving stone deterioration were identified by visual and SEM observations. Samples QX1, QX2, FL1, FL2, FL4, FL5, LY1, and LY2 showed similar morphological characteristics of microbial colonization, such as blocky or patchy white and green stains. The microstructures of these samples, as shown by SEM observations, revealed the presence of lichens on the stone surface, including the presence of characteristic cyanobacteria attached to fungal hyphae (Fig. 1A) and extensive fungal hyphal aggregates associated with diatom cells (Fig. 1B). Stone monuments tending to have a porous structure were extensively covered by green biofilm, which was likely caused by microorganisms such as cyanobacteria (arrow in Fig. 1C). Extensive microbial colonization present on samples FL3 and QX3 exhibited homologous morphological characteristics, e.g., colonization by white aggregates of microorganisms and inorganic minerals, but differences in microbial composition and microstructure were also found. In Fig. 1D and E, colonies are composed primarily of filamentous microorganisms in sample FL3 while clusters of spherical bacterial or cyanobacterial cells were embedded in layers of deposits and formed spheroidal or hemispheroidal aggregates (Fig. 1F). Surfaces of the no. 66 Bodhisattva statue exhibited a rough, brown colony morphology characteristic of microbial contamination. Deterioration pattern analyses of stone show that different microbial colonizers found on stone monuments are the most probable cause of observed esthetic damage since these colonizers are easily removed from the surface with sterilized water and a brush. However, the layers of deposits, likely caused by biomineralization of microorganisms and identified as calcium carbonate precipitation, are almost impossible to remove by traditional remediation techniques alone. Analysis of the composition of deposits revealed that the white stains from samples FL3 and QX3 were mostly composed of calcium carbonate, while calcium was absent from other samples tested by energy-dispersive spectroscopy (EDS) analysis (Fig. 1G to I).

DNA sequence data and alpha diversity. For general sequencing analyses of bacteria in both 2016 and 2017, 969,501 and 779,773 paired-end (PE) reads were generated from raw data and 697,857 and 625,728 high-quality sequences were obtained after filtering, respectively. The average length of valid sequences was 451 bp in 2016 and 434 bp in 2017. In both 2016 and 2017, a total of 730 bacterial operational taxonomic units (OTUs) were identified in all 24 samples, containing a subset of 28,767 sequences per sample. Samples from 2016 and 2017 harbored 46 and 24 unique OTUs, respectively (accounting for 6.3% and 3.3% of the total OTUs), while they had 660 OTUs in common. For general sequencing analyses of fungal samples in the 2016 and 2017 data sets, 808,647 and 696,528 PE reads were generated and 712,556 and 671,581 valid sequences were obtained by a chimera removal process, respectively. The average length of the valid sequences was 312 bp in 2016 and 314 bp in 2017, which was significantly shorter than the length of bacterial sequences. Besides, a total of 701 fungal OTUs comprising an average of 36,675 sequences in 24 samples contained 622 shared and 79 unique OTUs (32 for the 2016 data set and 47 for the 2017 data set). Rarefaction curve-based OTU abundance prediction, following clustering of sequences at 97% nucleotide identity, was used to standardize and compare observed taxon richness among samples and to determine whether the contents of intestinal segments were unequally sampled.

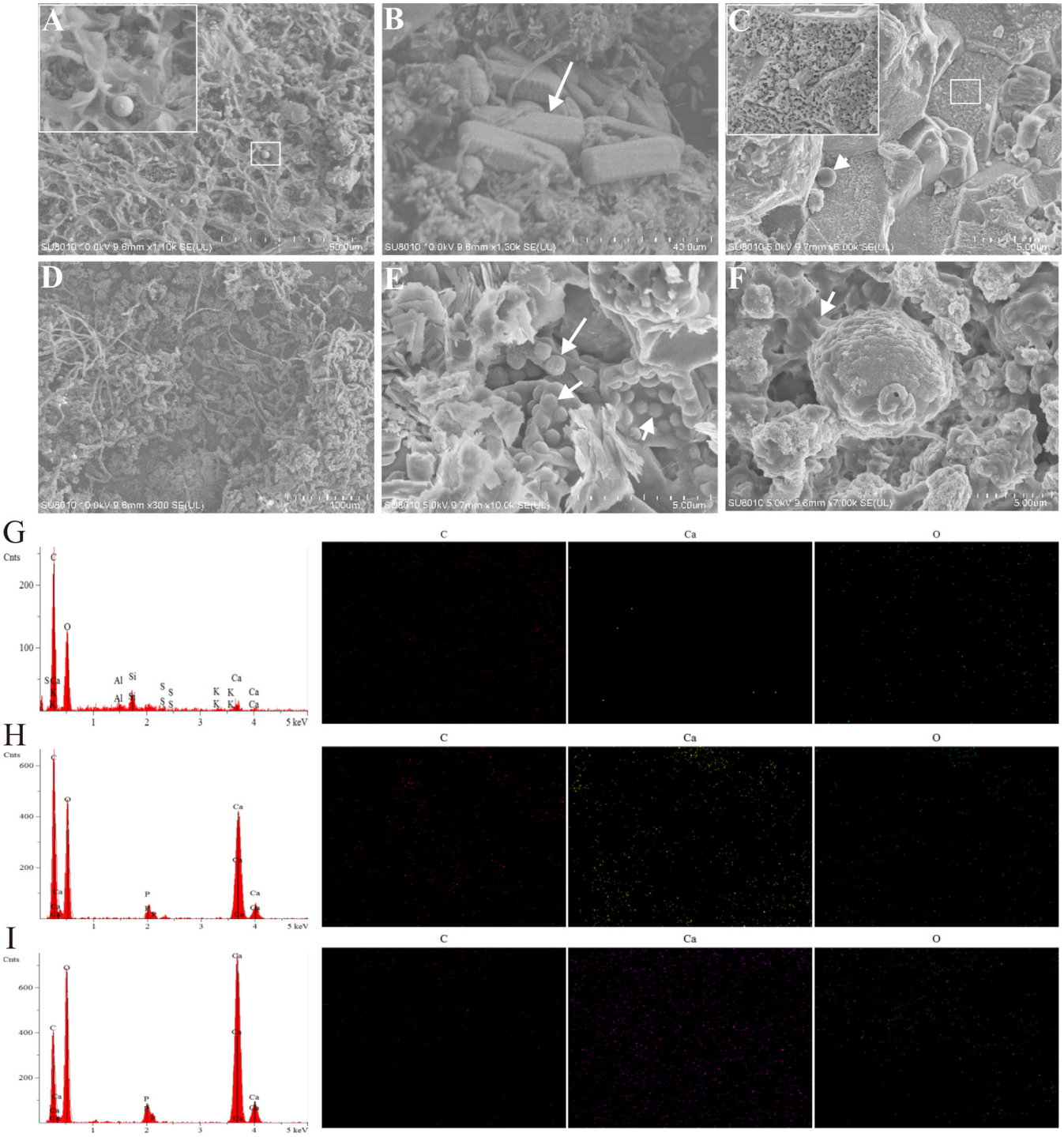

FIG 1 SEM images of microbial communities on different stone monuments. (A) Lichens and cyanobacterial cells on a stone surface. (B) Extensive fungal hyphal aggregates associated with diatom cells. (C) A porous structure is likely caused by microbial deterioration in QT1. (D) FL3 was increasingly colonized by actinomycete hyphae. (E, F) Signs of microbial colonization and spheroidal or hemispheroidal calcium carbonate precipitation and EPS. (G to I) Samples FL3 and QX3 were mostly composed of calcium carbonate, while calcium was absent from QX1 tested by EDS analysis.

The Chao 1 index was computed to determine the species richness of bacterial and fungal samples, as well as to determine whether richness differed among our 12 samples or between the 2 years in which data were collected. We found no consistent differences among samples. However, samples QX1 and QX3 showed a significant decrease in bacterial and fungal abundance from 2016 to 2017, while samples FL2, LY1,

QX2, and FL4 showed an increase. Moreover, samples FL1, FL3, QT1, FL5, and FL6 showed a significant decrease in bacterial abundance from 2016 to 2017. The Shannon and Simpson indexes were used to estimate species diversity, and from 2016 to 2017, most samples exhibited a consistent decrease in both indices, with the exception of samples QX2 and FL4, which showed an increase in bacterial communities from 2016 to 2017. Surprisingly, fungal diversity, as characterized by the two indices, showed a different trend, with an increase from 2016 to 2017 found in most samples but a decrease in samples QX2, QX3, LY2, and FL4. In summary, an increase and decrease in bacterial diversity corresponded to a decrease and increase in fungal diversity in most samples from 2016 to 2017. However, in samples LY2 and QX3, species diversity found in bacterial and fungal communities showed stronger synergy between the bacterial and fungal communities present.

Taxonomic assemblages of bacterial and fungal communities. The bacterial communities found in samples from 2016 and 2017 were classified as belonging to 18 different phyla, comprising 174 identified genera (Fig. 2). Samples from 2016 and 2017 exhibited similar distributions but different relative abundances of major bacterial phyla. Most samples were characterized as lichen-associated colonizers by visual and SEM observations, including QX1, QX2, FL1, FL2, FL4, FL5, LY1, and LY2. These samples contained a high relative abundance of cyanobacteria and proteobacteria. From 2016 to 2017, the bacterial composition of most of these samples varied strongly, as reflected by the increased abundance of cyanobacteria and the decreased abundance of proteobacteria, with the exception of samples LY2 and FL4, which showed a decrease in cyanobacteria and an increase in proteobacteria. Variation between cyanobacteria and proteobacteria exhibited significant interaction effects, and this trend was present in samples QT1 and FL6. Although deterioration in samples FL3 and QX3 exhibited similar morphological characteristics and microbial communities were correlated with calcium carbonate precipitation, we found differences in species diversity and richness. Actinobacteria were highly prevalent in sample FL3, where they composed 78.4% and 95.5% of all bacteria in 2016 and 2017, respectively. Proteobacteria were dominant in sample QX3, with an abundance in 2016 of 74.3%, but these were replaced by cyanobacteria as the predominant bacterial community in 2017. Other phyla, including *Acidobacteria* and *Bacteroidetes*, were found in all samples but did not show high relative abundance in general; however, they made up 24.9% of sample LY1 (*Acidobacteria*) and 22.1% of sample QT1 (*Bacteroidetes*). In addition, we identified five fungal phyla (Ascomycota, Basidiomycota, Zygomycota, Chytridiomycota, and Glomeromycota) in 1 or more of our 12 samples from 2016 and 2017. Ascomycota was the most abundant fungal community, with average abundances of 69 and 68.2% in 2016 and 2017, respectively, although this group varied drastically and irregularly in relative abundance from 2016 to 2017. Zygomycota, Chytridiomycota, Glomeromycota, and Basidiomycota were found only in individual samples in both 2016 and 2017 and accounted for a very small proportion of the total number of species found. Unidentified fungal communities showed an average abundance of 30.7% in 2016 and 31.2% in 2017, although in LY2, QT1, and FL6, the value was almost 65%.

Bacteria and fungi correlated with stone deterioration. The relative abundances and distributions of the 90 most abundant bacterial genera from 12 stone samples in 2016 and 2017 are shown. Remarkably, unclassified bacteria were found to have the highest relative abundance and accounted for an average of 59.2% of the bacteria in all samples. The most notable exception was sample FL3, which exhibited much lower abundances of 6.28 and 2.02% in the 2016 and 2017 data sets, respectively. *Crossiella*, which was likely the primary cause of $CaCO_3$ precipitation, was the dominant genus found in sample FL3, accounting for approximately 84% of the available bacteria. To comprehensively understand the interaction effects between core bacteria and stone deterioration, a network of significant co-occurrence and coexclusion relationships among genera was constructed on the basis of their correlation matrix (Fig. 3). Among the 129 bacterial families detected, the top 50 bacterial genera found in the population

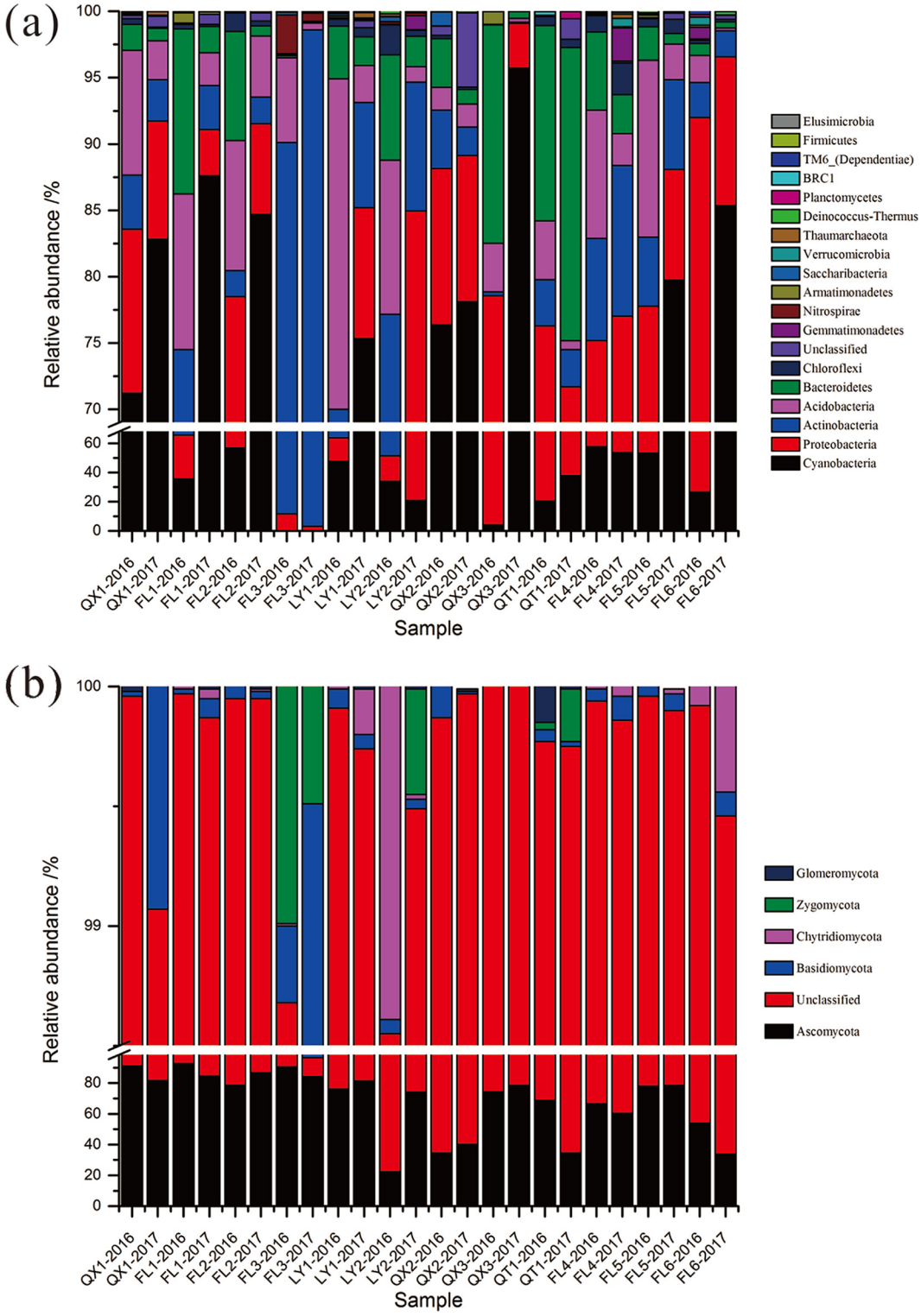

FIG 2 Distribution patterns of bacterial (a) and fungal (b) taxa in 2016 and 2017.

were used to construct this association network, of which 20 bacterial families with more than 87% relative abundance were deemed to be core bacteria. Members of the family *Methylobacteriaceae* were found to be strongly positively correlated with *Xylochloris irregularis* and members of the family *Micromonosporaceae*, a fact reflected by the high abundance of these bacterial families in almost all of the samples collected in

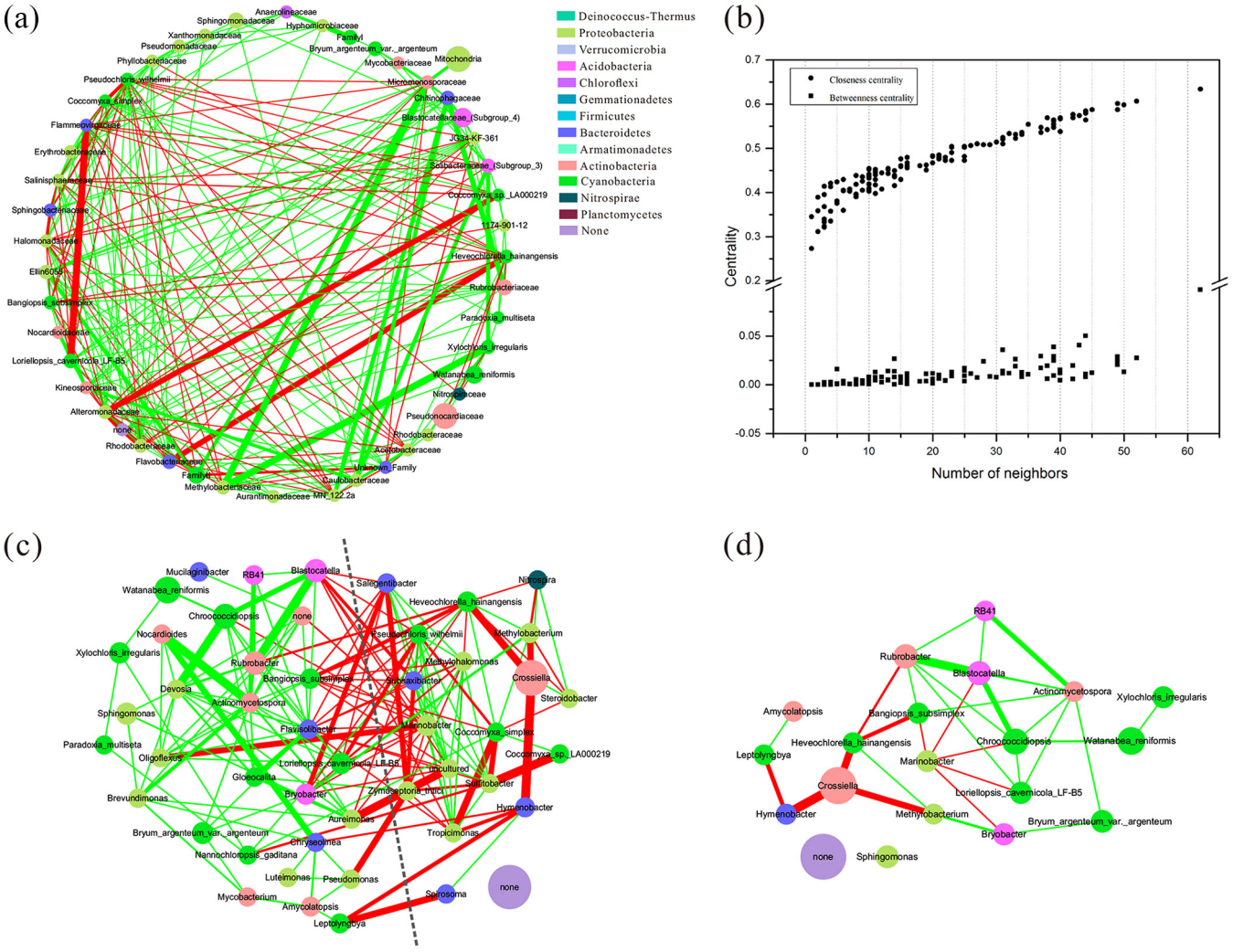

FIG 3 Co-occurrence network of significantly interacting bacterial families (a) and genera (c and d). Positively and negatively interacting bacterial families and genera are connected by green and red lines, respectively. The thickness of each line is proportional to the significance of the interaction (*q* value), and the size of the circle is proportional to the average relative abundance of bacterial families and genera. Panel b represents the bacterial families that were assigned to betweenness centrality and closeness centrality.

both 2016 and 2017. The presence of members of the family *Chitinophagaceae* was positively correlated with the presence of members of the families *Rubrobacteraceae* and *Caulobacteraceae*. The presence of members of the family *Solibacteraceae* (subgroup 3) was positively correlated with the presence of *X. irregularis* and members of the family *Caulobacteraceae*. The presence of *Loriellopsis cavernicola* LF-B5 was negatively correlated with the presence of members of the family *Flammeovirgaceae*, and members of the family *Flavobacteriaceae* were negatively correlated with the presence of *Heveochlorella hainangensis*. Nodes that had low betweenness centrality, as well as high mean degree and closeness centrality, were often considered to be potential keystone families; however, few such bacterial families were detected. Association networks were collapsed at the genus level to identify key network hubs associated with stone deterioration. Bacteria positively correlated with deterioration formed a complex network with strong interactions, while bacteria negatively correlated with deterioration exhibited a weak connection (Fig. 3C). Species of the genera *Bryobacter*, *Chroococcidiopsis*, *Rubrobacter*, *Blastocatella*, and *Sphingomonas*, as well as *L. cavernicola* LF-B5, were found in almost all samples and had a high relative abundance. These were defined as key hubs with strong correlations with deterioration. Remarkably, the genus *Crossiella* accounted for a majority of the bacterial communities in sample FL3

but was negatively correlated with the presence of other core genera, which was likely caused by inconspicuous abundances in other samples.

The fungal compositions of all 12 samples by genera, for all sites in both years, were determined, and the 40 most prevalent fungal genera were used to construct correlation networks. *Powellomyces* spp. were positively correlated with *Devriesia* and *Leptosphaerulina* spp. and negatively correlated with *Trichosporon* and *Lepraria* spp. Interestingly, the genus *Lepraria* was among the most abundant fungal communities but exhibited weak connections with other predominant fungal genera. *Lepraria*, along with *Mycosphaerella*, was negatively correlated with the presence of *Simplicillium* and *Cladosporium*, indicating that some fungal genera dominated only in individual samples. No significant and consistent correlation effects among relative abundance, closeness centrality, and betweenness centrality were shown in fungal communities. This could be due to the fact that samples contained dominant unclassified genera or to the possibility that the distribution of detected fungi was not randomly sampled.

Functional prediction of the deterioration-associated microbiome. PICRUSt software was used to analyze the KEGG pathway compositions of the deterioration-associated microbiome. The top 80 most abundant KEGG orthology pathways (Fig. 4) exhibited significant differences in the proportions of genes for photosynthesis and photosynthesis proteins between FL3 and other samples, which can probably be attributed to the low relative abundance of cyanobacteria in sample FL3. Additionally, proportions of genes for butanoate metabolism, propanoate metabolism, valine, beta-alanine metabolism, tryptophan metabolism, and fatty acid metabolism in sample FL3 were also higher than in other samples, as were the proportions of genes involved in leucine and isoleucine degradation, benzoate degradation, aminobenzoate degradation, and lysine degradation. The ABC transporter system was significantly elevated in the deterioration-associated microbiome, which may affect the complex exchange of amino acids, molecules, or iron complexes in densely accumulated bacterial communities (30). The bacterial community exhibited significantly increased relative abundances of genes for methane, starch, and sucrose metabolism, as well as carbon fixation. A high relative abundance of these genes is also present in photosynthetic organisms, and this increase is almost synergistic with cyanobacteria from 2016 to 2017. The genus *Nitrospira*, which had an abundance of 2.92% in sample FL3, probably contributed to an increase in the abundance of genes related to nitrogen metabolism. Moreover, we found genes involved in two system pathways: the bacterial chemotaxis sensor pathway and biofilm formation. Genes from both pathways were enriched in the microbiome, and both pathways are responsible for signaling, as they protect organisms from damage from the extracellular environment. Metabolic pathways involving nitrotoluene degradation, dioxin degradation, toluene degradation, polycyclic aromatic hydrocarbon degradation, chlorocyclohexane and chlorobenzene degradation, styrene degradation, and naphthalene degradation may be under selection to upregulate genes coding enzymes capable of degrading pesticides and persistent biodegradable organic pollutants. However, this degradation may affect stone monuments and is undesirable. Genes involving mineral absorption and calcium signaling pathways were found to be present in 24 samples of the microbiome and likely facilitated calcium carbonate precipitation in samples FL3 and LY3. Clusters of Orthologous Groups functional classification, which we used as a supplementary bacterial function prediction method, showed no significant change in any samples from 2016 to 2017. Some genes involving signal transduction, amino acid transport, energy production and conversion, carbohydrate metabolism, and transcription accounted for a relatively large proportion of the genes in 12 samples in both 2016 and 2017.

Across all of the fungal OTUs and valid sequences from the 2016 and 2017 data sets, three main trophic modes and eight guilds were successfully assigned to 138 OTUs by using FUNGuild (Fig. 5). A total of 85% of the fungal OTUs identified belonged to Ascomycota, while the other 15% were classified as Basidiomycota and Zygomycota. Wood saprotrophs known as white rot, soft rot, and brown rot fungi were also found

FIG 4 KEGG pathways enriched in epilithic bacterial communities. The relative abundances of pathways were compared among 12 samples in both 2016 and 2017.

in all of the fungal communities and were present in 54% of all observed OTUs. Lichenized fungi were present only in Ascomycota, while arbuscular mycorrhizal fungi were almost completely absent from the fungal genera, with the exception of OTU 643 (*Acaulospora*). Additionally, the distribution and variation characteristics of fungal guilds, which were broadly defined on the basis of trophic modes, were evaluated

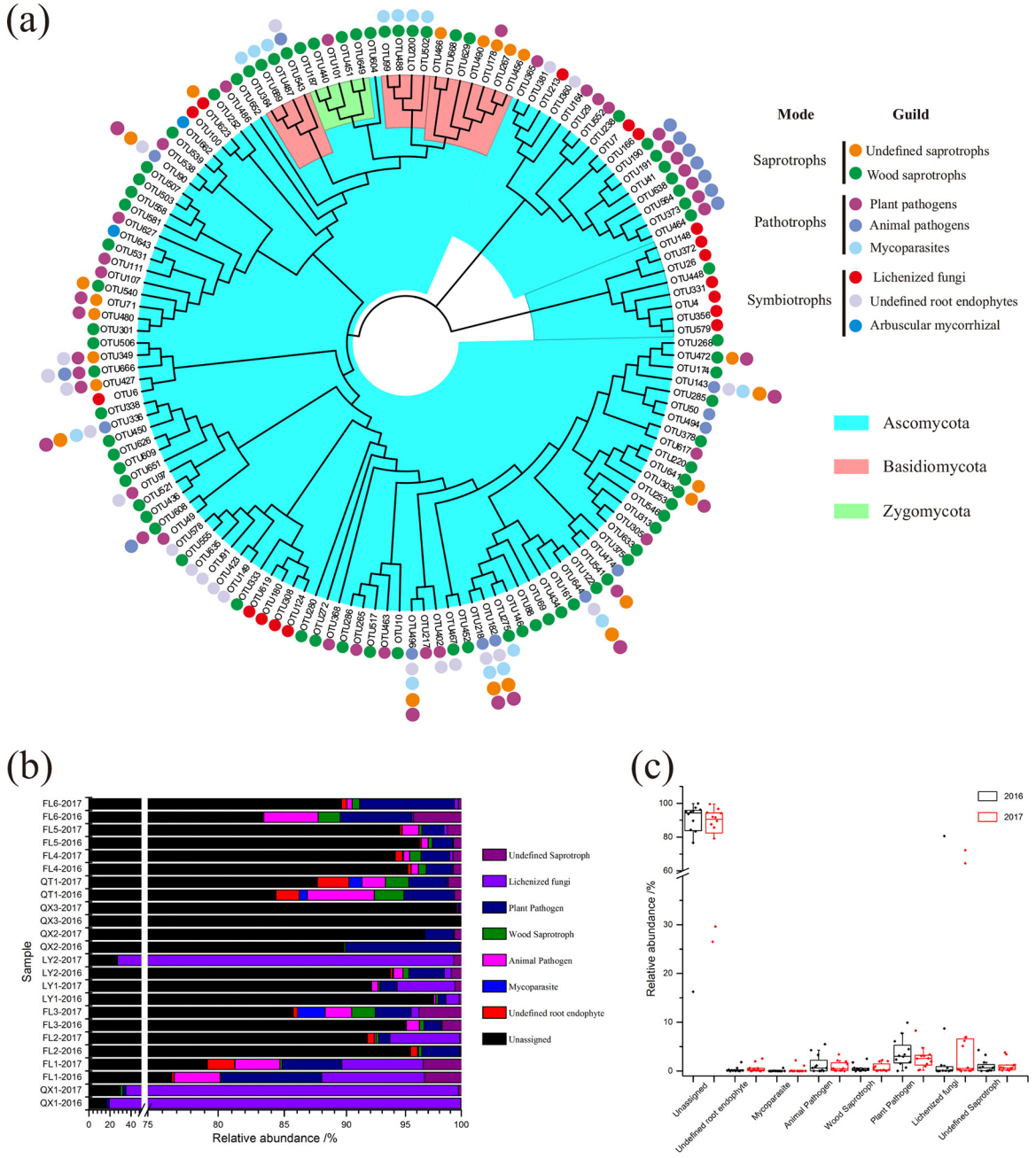

FIG 5 Guild assignments of 138 identified OTUs (a) and variation in fungal community composition (b, c). OTUs and sequences not assigned to guilds were placed in the unassigned group.

among all stone samples from 2016 and 2017 (Fig. 5b and c). Unassigned guilds were the largest fungal group found in our samples, with a mean relative abundance of 82.9%. This group was, however, absent from sample QX1. When unassigned OTUs were excluded, lichenized fungi were the largest guild in valid sequence richness. Along with the lichenized fungi, members of six other guilds, including plant pathogens, undefined saprotrophs, animal pathogens, wood saprotrophs, undefined root endophytes, and mycoparasites, were also detected in 12 samples in both 2016 and 2017.

Biomineralization of culturable microbes. Bacterial and fungal strains were isolated from 12 stone monuments by a culture-dependent approach. All bacterial and fungal isolates were sequenced and grouped by using PCR amplification of 16S rRNA genes and internal transcribed spacer (ITS) regions. This method produced species-

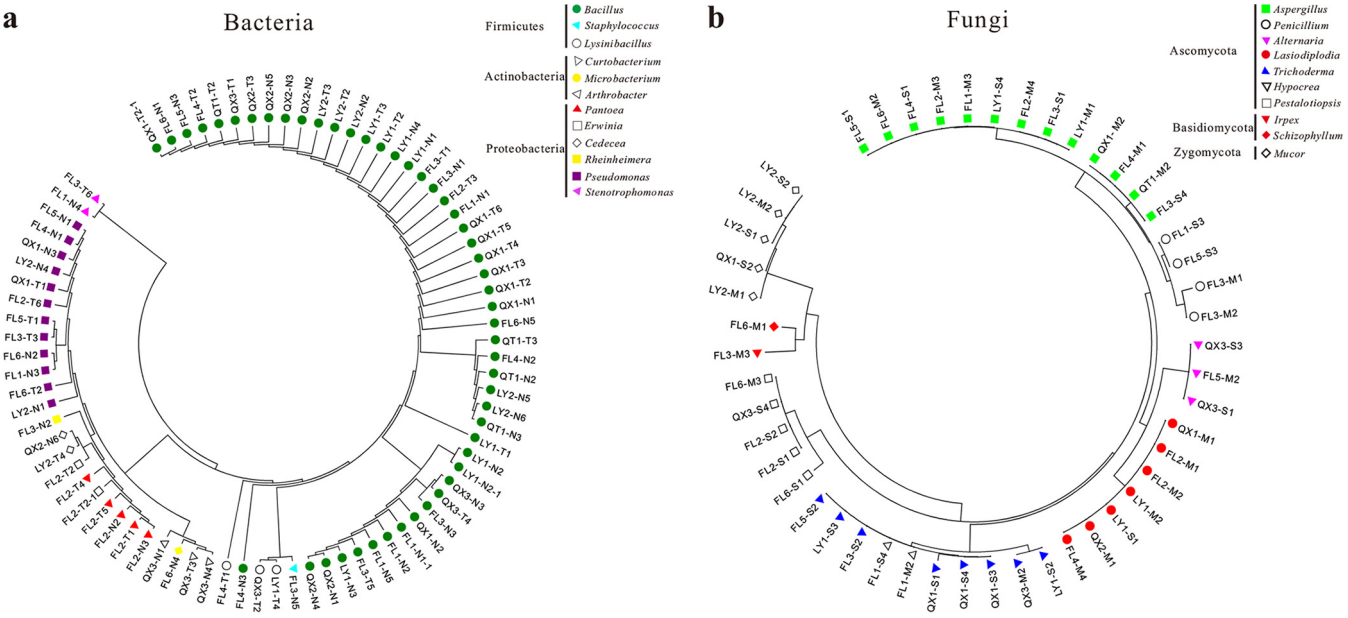

FIG 6 Bacterial and fungal strains were isolated from 12 samples.

specific profiles, which allowed the bacteria to be divided into 85 clusters and the fungal strains to be divided into 49 clusters. Of the 85 bacterial strains cultivated from stone monuments, 56 belonged to the phylum *Firmicutes*, which includes *Bacillus*, *Staphylococcus*, and *Lysinibacillus*. In addition, 25 bacterial isolates were found to belong to the *Proteobacteria*, including *Pseudomonas*, *Stenotrophomonas*, *Pantoea*, *Erwinia*, *Rheinheimera*, and *Cedecea*; these accounted for 29% of the strains isolated. *Arthrobacter*, *Curtobacterium*, and *Microbacterium* belong to the *Actinobacteria*, and each represented approximately 1% of the bacterial isolates (Fig. 6). The fungal community isolated from stone was substantially more diverse. Several strains belonged to the phylum Ascomycota, including species of the genera *Lasiodiplodia* (14%), *Aspergillus* (26%), *Trichoderma* (16%), *Hypocrea* (4%), *Penicillium* (8%), *Pestalotiopsis* (10%), and *Alternaria* (6%). Other isolates belonged to the Zygomycota and Basidiomycota and were identified as species of the genera *Mucor*, *Irpex*, and *Schizophyllum*.

Three different precipitation assays were used to screen $CaCO_3$ precipitations for isolated bacterial strains. These used B-4 agar, M-3 agar, and B-4 liquid medium. A total of 64% of the bacterial isolates showed $CaCO_3$ precipitation activity in at least one of the plate assays. Fifty-four of the 85 bacterial isolates recovered from stone samples produced positive reactions in B-4 agar and liquid medium assays, while 50 of the 85 isolates showed positive reactions on M-3 agar. Several isolates, including FL1-N4 (*Stenotrophomonas maltophilia* NBt8_50S), LY2-T1 (*Bacillus* sp. strain E-K49), FL2-T2 (*Erwinia* sp. strain DE003), and FL4-T1 (*Lysinibacillus* sp. strain E15), could form $CaCO_3$ crystals in B-4 medium but not on M-3 agar. Bacterial isolates that could form $CaCO_3$ crystals in B-4 medium included *Bacillus cereus*, *Stenotrophomonas maltophilia*, *Erwinia* sp., *Pseudomonas moraviensis*, *Rheinheimera* sp., *Lysinibacillus sphaericus*, *Pseudomonas* sp., *Cedecea* sp., *Bacillus thuringiensis*, *Bacillus marisflavi*, and *Pseudomonas rhodesiae*. $CaCO_3$ crystals formed on the surface of bacterial isolates in B-4 medium and on M-3 agar after incubation for 20 days are visible and differ in morphology. After 10 days of incubation with *B. cereus* (FL4-T2), spheroidal $CaCO_3$ crystals were found on the surface of B-4 agar, and this process is probably facilitated by EPS produced by bacterial isolates by entrapping and serving as a nucleation site. Moreover, EPS also increase the size of $CaCO_3$ deposits by mixing other precipitation and bacterial cells, forming a calcium carbonate-EPS (cell) mixture (Fig. 7). Deposits induced by bacterial isolates were identified and confirmed by EDS, X-ray diffraction, and fluorescent calcein staining

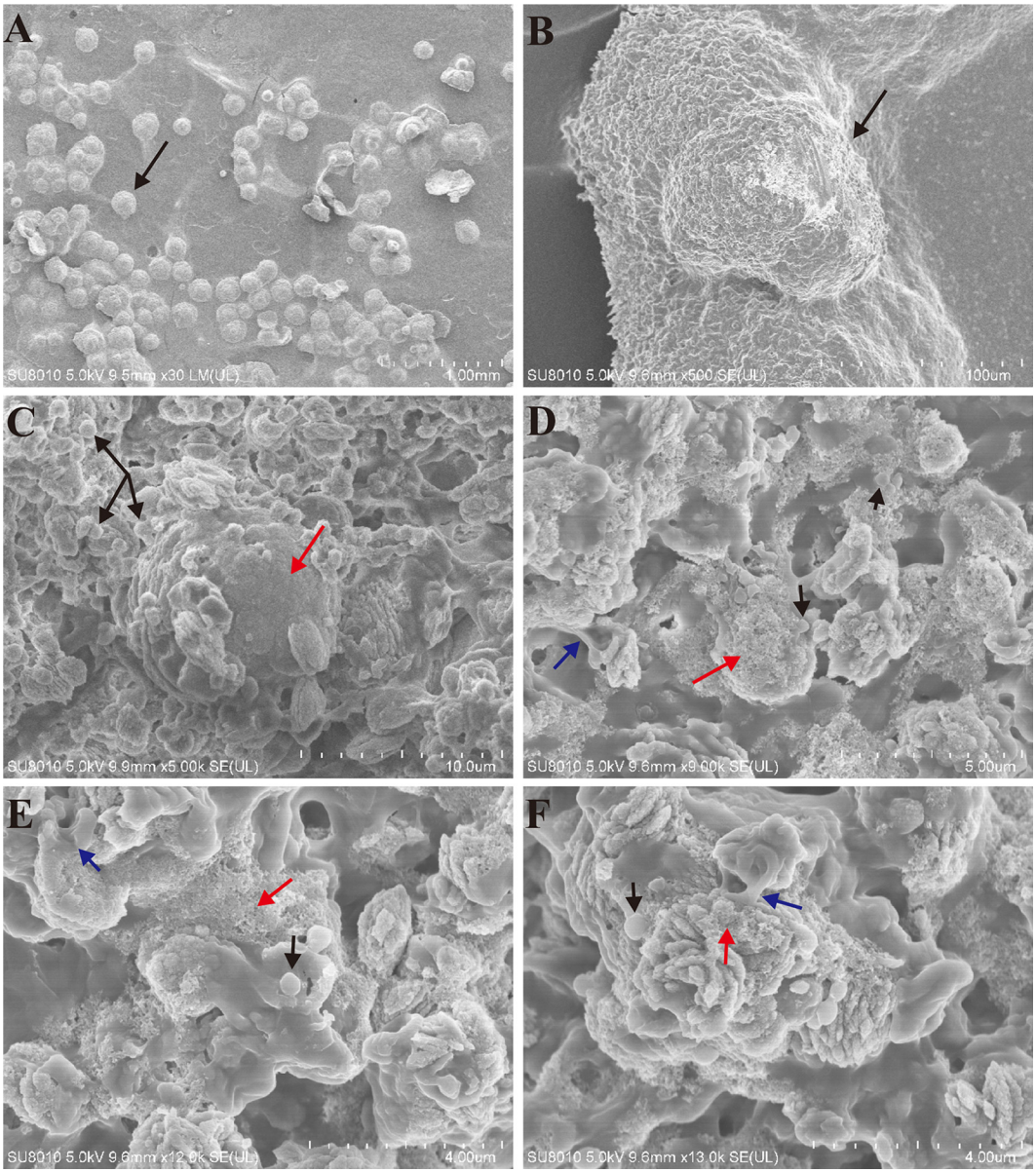

FIG 7 Relationship between bacterial isolates and $CaCO_3$ precipitation. (A, B) Spheroidal $CaCO_3$ crystals (black arrows) formed on the surface of B-4 agar incubated in the presence of *B. cereus* (FL4-T2) after 10 days. (C to F) Relationships among bacterial cells (black arrows), $CaCO_3$ precipitation (red arrows), and EPS (blue arrows).

analyses. $CaCO_3$ precipitation was successfully labeled with calcein and then visualized via fluorescent staining, with the biofilm itself remaining unstained (Fig. 8).

DISCUSSION

Comprehensive analyses of the microbiomes associated with deterioration of stone monuments may contribute to the understanding of mechanisms of deterioration, as well as to the identification of potentially beneficial or undesirable microbial communities and their genomic pathways. This information may provide a basis for the removal of deterioration-associated microorganisms and the application of beneficial species involving biomineralization for preservation of stone monuments. We defined the morphological structure of stone deterioration by visual and microstructural observations, mainly by observing plaque on the surface and white deposits. Surprisingly, white aggregates were composed mainly of cyanobacterial and bacterial cells, hyphae of actinomycetes, and calcium carbonate crystals, while other samples obtained from

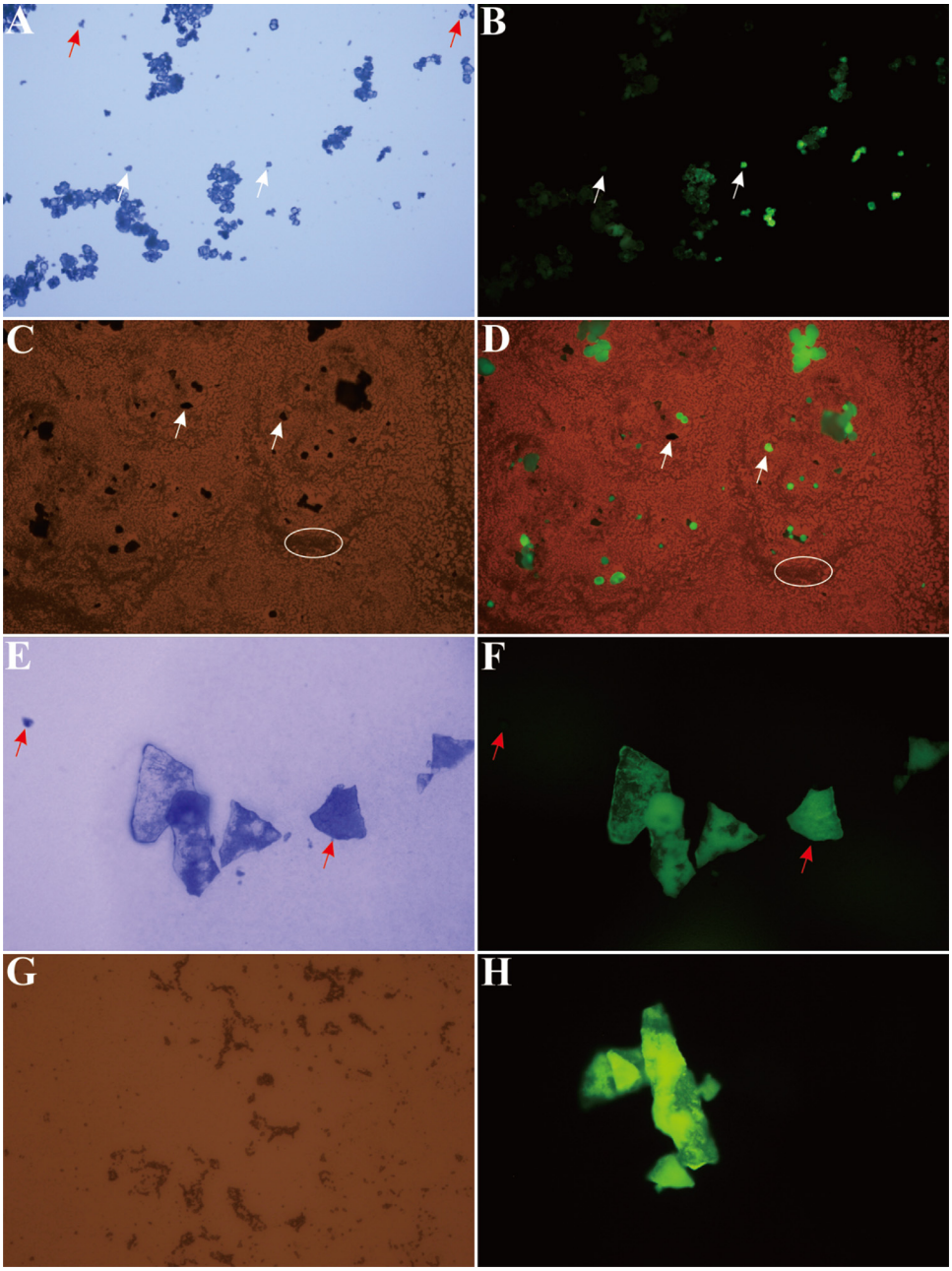

FIG 8 Observation of calcein incorporation into $CaCO_3$ precipitate with a fluorescence microscope (blue light excitation, green fluorescence emission). $CaCO_3$ crystals imaged by calcein staining appear green. (A) Abiotic $CaCO_3$ crystals observed with an optical microscope as an unstained control. (B) Fluorescent image of the position shown in panel A after staining with calcein. (C) Optical microscopic image of bacterial isolates after incubation on B-4 agar for 10 days. The white arrow indicates $CaCO_3$ crystals. The white ellipse indicates bacterial isolates. (D) Fluorescent image of the position shown in panel C after staining with calcein. Most $CaCO_3$ crystals were stained with calcein (green), although calcein cannot be incorporated into some bacterial cells (white ellipse). (E, F, H) Local observation of $CaCO_3$ precipitation before and after staining with calcein. (G) Fluorescence microscopic image of bacterial isolates incubated on modified B-4 agar (without Ca^{2+}) for 10 days without $CaCO_3$ precipitate formation.

well-separated geographic locations merely exhibited microbial colonization of the stone surface. These findings are consistent with reports on other stone monuments (4, 29, 31) indicating that stone monuments are particularly susceptible to esthetic and structural damage.

We defined the taxonomic structure of epilithic microbiota, comprising cyanobacteria, *Proteobacteria*, *Actinobacteria*, *Acidobacteria*, and *Bacteroidetes* in the bacterial

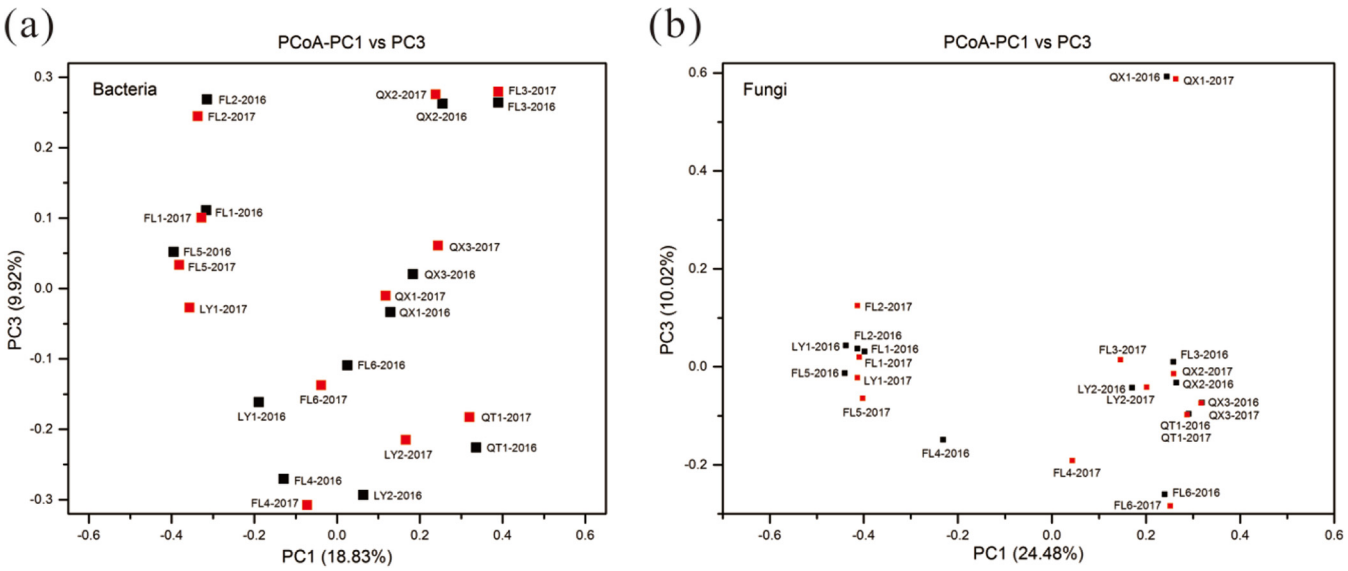

FIG 9 PCoA of bacterial (a) and fungal (b) communities.

community, as well as Ascomycota in the fungal community. Species richness characterized by the Chao 1 index exhibited no consistent increase or decrease among bacterial or fungal samples from 2016 to 2017. However, the synergetic effects are also present in the species diversity of bacterial and fungal communities. This is reflected by the fact that the Shannon and Simpson indexes increased and/or decreased in response to increases or decreases in 10 of the 12 samples from 2016 to 2017, while samples LY2 and QX3 showed coincident change. Additionally, principal-coordinate analysis (PCoA) revealed that the microhabitat, rather than the geographic location, was the major factor affecting the microbiome (Fig. 9). Although our 12 samples were collected at well-separated geographic locations, no substantial differences in the composition of the microbial populations were observed. In both 2016 and 2017, microbiome data from the same sampling point showed a consistent species composition, even when species abundance varied. Cyanobacteria were the most prevalent bacterial community among all samples from 2016 and 2017, with the exception of sample FL3, which was significantly dominated by a large proportion of actinobacteria. This result was consistent with the general rules of microbial establishment; i.e., cyanobacteria are most strongly associated with abundant sunshine and actinobacteria are commonly present in subterranean environments (32–35). Most samples, including QX1, FL1, FL2, LY1, QX2, QX3, QT1, FL5, and FL6, showed an increase in the relative abundance of cyanobacteria from 2016 to 2017, although this trend was not present in samples LY2 and FL4. Significant variation in the relative abundance of cyanobacteria was also found in sample QX3, which changed from 3.88% to 96.75% within a year. Coincidentally, changes in microbial composition can be reflected by sample features; for example, the sample from 2017 was also characterized as cyanobacterial or algal colonization (green biofilms after removal of $CaCO_3$ deposits) while a dry and rough plaque cover but without green biofilms was found in 2016. We also found the fungal composition to be less diverse than the bacterial composition, but greater variation was observed among different samples in 2016 and 2017.

pk;4We analyzed the association between the deterioration characteristics of each sample and the corresponding bacterial and fungal microbiota. Through this process, we found strong positive and negative correlations among different species in separate samples, such as the families *Pseudonocardiaceae* and *Blastocatellaceae*, which accounted for 92.37% in FL3 and 24.2% in LY1 but had no significant interaction with other families. Positive co-occurrence patterns of the families *Rubrobacteraceae*, *Methylobacteriaceae*, and *Chitinophagaceae* do not necessarily represent facilitative or mutu-

alistic interactions because of the low abundances in all bacterial communities. Association networks collapsed to the genus level showed a positive correlation pattern with strong and complex connections, as well as a negative correlation with loose and simple connections. Most of these genera belong to the *Cyanobacteria*, *Proteobacteria*, and *Actinobacteria*, which are identified as potential keystone taxa and contribute to stone deterioration. *Lepraria*, *Botryolepraria*, *Cladonia*, and *Devriesia* were the top four classified genera in terms of relative abundance and accounted for a large proportion of many individual samples. However, these genera also showed mutually exclusive interactions with others. We found that a large number of metabolic pathways related to photosynthesis proteins, photosynthesis, carotenoid biosynthesis, photosynthesis-antenna proteins, carbon fixation pathways in prokaryotes, and cyanoamino acid metabolism were enriched in the microbiota of the stone surface. While many metabolic pathways involve mineral absorption, calcium signaling, EPS production, fatty acid metabolism and membrane transport protein activities were enriched in the microbiome samples FL3 and LY3, and this enrichment probably involves the process of $CaCO_3$ precipitation (16). For the ecologically meaningful fungal categories, we found that the results matched well with our expectations about which guilds were probably enriched in each data set. When unassigned OTUs were excluded, lichenized fungi were considered to be the largest guild in most samples but were also absent from QX3. This finding was consistent with our hypothesis that fungi are symbiotically associated with cyanobacteria or alga-forming lichened stone, on which *Lepraria*, *Cladonia*, and *Botryolepraria* may play critical roles in microbial assembly.

The culture-dependent method is also able to detect spore-forming bacteria. For example, *Bacillus* spp. accounted for 61.2% of the species detected by using enrichment cultures but $<$0.01% of the sequences detected by high-throughput sequencing. This discrepancy is likely due to the reduced susceptibility of spores to DNA extraction. The most predominant fungal groups found belonged to the Ascomycota, as determined by both enrichment cultures and culture-independent techniques. Bacterial and fungal abundances were inconsistent according to different detection methods; we followed the general rule of cultivation-based methods, which assumes that cultures enable the detection of only 1 to 5% of the total microbial community (36). Highly diverse bacterial species have been reported to have the ability to induce $CaCO_3$ precipitation, of which *Bacillus* and *Pseudomonas* are the most common (17, 18, 28, 37). In our experiments, B-4 agar, M-3 agar, and B-4 liquid medium were used to detect the $CaCO_3$ precipitation activities of bacterial isolates, with 64% of the isolates showing positive reactions. Thirty-nine of 52 *Bacillus* and 5 of 13 *Pseudomonas* isolates showed $CaCO_3$ precipitation after inoculation onto agar or into liquid medium. Additionally, *Stenotrophomonas*, *Erwinia*, *Rheinheimera*, *Lysinibacillus*, and *Cedecea* have all been proven to form $CaCO_3$ deposits under experimental conditions. Considering the complexity of the interactions between microbiota and environments *in situ*, more data are needed to substantiate the conclusion that culturable bacteria can induce the formation of calcium carbonate on stone monuments. Finally, we note that bacterially induced carbonate mineralization is a novel, environmentally friendly approach to the conservation of stone and can be used with bacterial self-inoculation. This technique is effective because it can form exceptionally strong hybrid cement (29); this technique thereby provides a basis for the application of carbonatogenic bacteria for the protection of stone artworks.

MATERIALS AND METHODS

Site description and sampling. A total of 12 stone specimens were recovered from stone monuments located in the vicinity of the UNESCO World Heritage Site at the West Lake Cultural Landscape of Hangzhou. Samples QX1, QX2, and QX3 were collected from Qingxing palace. Sample QX1 was taken from the base of the pavilion, where there were signs of severe microbial deterioration, while samples QX2 and QX3 were collected from brown and black colonizers present on dragon carvings on a column pedestal made of white marble. Samples LY1 and LY2 were taken from the pagoda in the Lingyin temple. Sample QT1 was collected from the Qiantang gate. The other six samples were taken from the Klippe statues, of which there are more than 470 dating from the Five Dynasties to the Song (960 to 1279 AD) and Yuan (1271 to 1368 AD) dynasties. Samples FL1 and FL2 were collected from the head of a Buddhist statue and the bottom of a tower, respectively; Sample FL3 was collected from the surface of a statue

in the Longhong Cave; Sample FL4 was collected from Bodhisattva statue 63, which is located on a hillside. FL5 and FL6 were collected from Bodhisattva statues 61 and 66 on the same hillside. All samples were collected separately in 2016 and 2017 and scraped by scalpel as intact and aseptically as possible.

DNA extraction and 16S rRNA gene and ITS region sequencing. Total genomic DNA was extracted from the microbial samples with the Power Soil DNA isolation kit in accordance with the manufacturer's instructions. DNA samples were quantified with a Qubit 2.0 fluorometer (Invitrogen, Carlsbad, CA), and DNA quality was checked on a 0.8% agarose gel. Thirty to 50 ng of total DNA was used to generate amplicons with a MetaVx library preparation kit (Genewiz, Inc., South Plainfield, NJ, USA). For bacterial 16S rRNA gene sequencing, a panel of primers designed by Genewiz for relatively conserved regions bordering the V3, V4, and V5 hypervariable regions was used to generate amplicons for subsequent taxonomic analysis. The V3 and V4 regions were amplified with forward primers containing the sequence CCTACGGRRBGCASCAGKVRVGAAT and reverse primers containing the sequence GGACT ACNVGGGTWTCTAATCC. The V4 and V5 regions were amplified with forward primers containing the sequence GTGYCAGCMGCCGCGGTAA and reverse primers containing the sequence CTTGTGCGGKCCCC CGYCAATTC. For fungal ITS sequencing, two pairs of primers were designed to amplify conserved ITS regions. This amplification used a forward primer containing the sequence ACCTGCGGARGGAT and a reverse primer containing the sequence GAGATCCRTTGYTRAA for the ITS1 region and a forward primer containing the sequence GTGAATCATCGARTC and a reverse primer containing the sequence TCCTCCGCT TATTGAT for the ITS2 region. First-round PCR products were used as templates for second-round amplicon enrichment PCR. These primers also contained indexed adaptor sequences to permit uniform amplification of the library for downstream next-generation sequencing on an Illumina MiSeq instrument.

DNA libraries were validated by an Agilent 2100 Bioanalyzer (Agilent Technologies, Palo Alto, CA, USA) and quantified by Qubit and real-time PCR (Applied Biosystems, Carlsbad, CA, USA). DNA libraries were multiplexed and loaded onto an Illumina MiSeq instrument in accordance with the manufacturer's instructions (Illumina, San Diego, CA, USA). Sequencing was performed by using a 2-by-300/250 PE configuration; image analysis and base calling were conducted with the MiSeq Control Software embedded in the MiSeq instrument.

Statistical analysis. The QIIME data analysis package was used to analyze 16S rRNA gene and ITS sequence data, and processing was carried out as follows. Forward and reverse reads were joined, assigned to samples, and then truncated by cutting off the primer sequence. Quality filtering of joined sequences was performed, and sequences that had $<$200 bp, no ambiguous bases, or a mean quality score of $\geq$20 were discarded. To detect chimeric sequences, the remaining sequences were compared to the reference (RDP Gold) database by using the UCHIME algorithm and all chimeric sequences were removed. All remaining sequences were used in the final analysis. Bacterial sequences were grouped into OTUs by using the clustering program VSEARCH (1.9.6) against the Silva 119 database, preclustered at 97% sequence identity, while fungal sequences were grouped into OTUs with the clustering program VSEARCH (1.9.6) against the UNITE ITS database (https://unite.ut.ee/). The Ribosomal Database Program (RDP) classifier was used to assign a taxonomic category to all OTUs at a confidence threshold of 0.8. The RDP classifier uses the Silva 119 database and the UNITE ITS database, which has taxonomic categories predicted to the species level. Sequences were rarefied prior to calculation of alpha and beta diversity statistics. Alpha diversity indexes were calculated in QIIME from rarefied samples; the Shannon index was used for diversity, and the Chao 1 index was used for richness. Beta diversity was calculated by using weighted and unweighted UniFrac. Finally, PCoA was performed.

Microbial co-occurrence networks. The association of biodeterioration phenotypes with epilithic communities of stone monuments was evaluated by using the bacterial and fungal community data. In the community data matrix, only those bacterial and fungal orders whose sum of sequencing reads in all data sets was $>$200 were included in the co-occurrence networks. To reveal signs of potential positive and negative interactions between any two marker OTUs, a co-occurrence adjacency matrix was constructed by calculating and standardizing bacterial and fungal community relative abundance in stone samples by using Cytoscape 3.5.1 configured by using the CoNET algorithm (38, 39). This yields a value between 0 (no co-occurrence in any samples) and 1 (perfectly overlapping profiles of species occurrence). Node size corresponded to the average relative abundance of bacterial and fungal orders, while the thickness of edges represented the significance of the interaction (*q* values) after thresholding. Additionally, the closeness and betweenness centrality, representing the significance of a node, were measured by NetworkAnalyzer, and potential keystone orders were recognized by those nodes with high closeness centrality and low betweenness centrality (40).

Microbial function prediction. PICRUSt software was used to predict the metagenome functional genotype of microbiota colonizing stone monuments by analyzing bacterial 16S rRNA gene sequences (41). Valid OTUs were picked against a reference data set for closed-reference OTU picking with OTUs assigned at 97% identity, followed by an alignment with the Greengenes database and normalization to OTU abundance data sets on the basis of predicted 16S rRNA gene copy numbers. Finally, the predicted metagenome functional content of the microbial community was obtained by comparing closed OTUs with corresponding KEGG and EggNOG functional genes and genome statistics (42).

Fungal functional prediction was performed with FUNGuild software, a tool that can be used to annotate the functional guild classification of fungal OTUs by ecological guild independently of a sequencing platform or analysis pipeline (43, 44). Because less genome information is available for fungi than for the bacterial community, the functional annotations of OTUs are often limited to three broad groupings, pathotrophs, symbiotrophs, and saprotrophs, referred to as trophic modes, and it is often not possible to effectively parse OTUs into functional genes and metabolic pathways. Furthermore, a total of 12 detailed categories were identified as guilds. These included animal pathogens, plant pathogens, and

mycoparasites as pathotrophs; wood saprotrophs and undefined saprotrophs as saprotrophs; and arbuscular mycorrhizal fungi, ectomycorrhizal fungi, ericoid mycorrhizal fungi, foliar endophytes, lichenicolous fungi, and lichenized fungi as symbiotrophs (45–47).

Microbial strain isolation and identification. Approximately 20 mg of the sampled material was inoculated into four sterilized media, of which two were bacterial media containing nutrient agar (NA) and Trypticase soy agar (TSA) supplemented with 50 mg · liter^{-1} cycloheximide. The other media were designed for culturing of fungi and contained malt extract agar (MEA) and Sabouraud glucose agar (SGA) with 100 mg · liter^{-1} chloramphenicol and streptomycin. The compositions of the different media were as follows. NA medium contained peptone at 10 g/liter, beef extract at 3 g/liter, NaCl at 5 g/liter, and agar at 15 g/liter (pH 7.3). TSA medium contained Tryptone at 15 g/liter, peptone from soybeans at 5 g/liter, NaCl at 5 g/liter, and agar at 15 g/liter (pH 7.3). MEA medium contained malt extract at 130 g/liter, chloramphenicol at 0.1 g/liter, and agar at 15 g/liter (pH 6.0). SGA medium contained peptone at 10 g/liter, glucose at 40 g/liter, and agar at 15 g/liter (pH 5.6). Medium plates were incubated at 30°C for 7 days. Each culture assay was performed in duplicate. When growth of microbial strains became apparent, the strains were transferred to a fresh plate for selection of pure colonies. Finally, colonies macroscopically different in appearance were selected for identification to the species level and biomineralization assays.

Microbial DNA extraction was performed in accordance with a cetyltrimethylammonium bromide method designed to extract DNA from plant cells (48). The genome was used as a template for 16S rRNA gene and ITS region amplifications. Bacterial 16S rRNA gene sequences were amplified with universal primers 341f (5′-CCTACGGGAGGCAGCAG-3′) and 907r (5′-CCCCGTCAATTCATTTGAGTTT-3′) (49). The fungal ITS region was amplified with universal primers ITS1 (5′-TCCGTAGGTGAACCTGCGG-3′) and ITS4 (5′-TCCTCCGCTTATTGATATGC-3′) (50). The PCR mixture (50 μl) consisted of 4 U of *Taq* polymerase, 5 μl of PCR buffer, 0.2 μM each primer, 200 μM deoxynucleoside triphosphates, 10 ng of template DNA, and sterile ultrapure water to 50 μl. The PCR cycling protocol was as follows: initial denaturing at 94°C for 3 min, followed by 30 cycles of 94°C for 1 min, annealing at 53°C (bacteria) or 55°C (fungi) for 1 min, and extension for 1 min at 72°C, with a final extension for 10 min at 72°C. To identify isolated bacterial and fungal strains, the sequences obtained were used to run BLAST searches against the GenBank database (National Center for Biotechnology Information [NCBI]).

Biomineralization assays. For inoculum preparation, all of the bacterial species isolated in this study were precultured in liquid LB medium (10 g of NaCl, 5 g of yeast, 10 g of peptone, 1,000 ml of sterile distilled water, pH 7.2). Each culture was incubated at 30°C on a shaker for 24 h and then diluted in sterilized ultrapure water to a final optical density at 600 nm of 0.01 for inoculation into B-4 liquid medium or onto B-4 agar or M-3 agar. B-4 medium contained (per liter) 2.5 g of calcium acetate, 4.0 g of yeast extract, and 10 g of glucose, all adjusted to pH 8.0 with NaOH (18, 26, 51). M-3 agar contained 1% Bacto casitone, 1% calcium acetate, and 0.2% K_2CO_3 in distilled water, all adjusted to pH 8.0 (51, 52). All bacterial strains were incubated at 30°C for up to 20 days under standing- and shaking-culture conditions. Experiments were carried out in triplicate; controls consisted of uninoculated agar or medium and heat-killed bacteria. Precipitated crystals on solid agar and in liquid medium were collected as described previously (37). Precipitates were obtained by filtration through a 0.45-μm Millipore filter. Crystals were washed with sterile distilled water and dried at 50°C overnight. Precipitates were analyzed by SEM-EDS, X-ray diffraction, and fluorescence imaging techniques.

A series of experiments were carried out by using calcein staining to determine the calcium content of crystal precipitate. Calcein, which is a fluorescent calcium indicator that binds to calcium and calcium ions, is incorporated into growing calcium carbonate crystals (53–56). In experiments with calcein fluorescent staining of *in situ* calcium carbonate precipitate, we used a concentrated solution of calcein at 2 g · liter of distilled water^{-1} buffered to pH 6 with sodium bicarbonate to enhance solubility (54). This concentrate was then added to filtered seawater (0.2-μm-pore-size filter) and adjusted to pH 8.2 with NaOH; this produced a marking solution containing a final calcein concentration of 100 μM. This concentration was chosen because it was found to be optimal for staining in previous experiments. Observations were made with a Nikon Eclipse Ti inverted microscope (Tokyo, Japan) and a C-SHG 1 mercury lamp (Nikon, Tokyo, Japan). Samples were excited with pure blue light, and fluorescence emission was detected with a LH-M100CB-1 digital camera (Nikon).

Accession number(s). Raw sequences obtained in this study have been deposited in the NCBI Sequence Read Archive database under accession numbers SRP114654 and SRP116627.

ACKNOWLEDGMENTS

This work was supported by the National Innovation League (Zhejiang Province) in Cultural Heritage Conservation Science and Technology (grant [2015] 878), the Conservation Science and Technology Project of Zhejiang Provincial Administration of Cultural Heritage (2015), and the Conservation Science and Technology Research Project of Outstanding Youth (grant [2015] 299).

We have no conflicts of interest to declare.

REFERENCES

1. Ciferri O. 1999. Microbial degradation of paintings. Appl Environ Microbiol 65:879–885.
2. Sterflinger K, Pinar G. 2013. Microbial deterioration of cultural heritage and works of art—tilting at windmills? Appl Microbiol Biotechnol 97:9637–9646. https://doi.org/10.1007/s00253-013-5283-1.
3. Warscheid T, Braams J. 2000. Biodeterioration of stone: a review. Int

Biodeterior Biodegradation 46:343–368. https://doi.org/10.1016/S0964-8305(00)00109-8.
4. Cutler NA, Chaput DL, Oliver AE, Viles HA. 2015. The spatial organization and microbial community structure of an epilithic biofilm. FEMS Microbiol Ecol 91:fiu027. https://doi.org/10.1093/femsec/fiu027.
5. Saiz-Jimenez C, Miller AZ, Martin-Sanchez PM, Hernandez-Marine M. 2012. Uncovering the origin of the black stains in Lascaux Cave in France. Environ Microbiol 14:3220–3231. https://doi.org/10.1111/1462-2920.12008.
6. Scheerer S, Ortega-Morales O, Gaylarde C. 2009. Microbial deterioration of stone monuments—an updated overview. Adv Appl Microbiol 66:97–139. https://doi.org/10.1016/S0065-2164(08)00805-8.
7. Crispim CA, Gaylarde PM, Gaylarde CC, Neilan BA. 2006. Deteriogenic cyanobacteria, on historic buildings in Brazil detected by culture and molecular techniques. Int Biodeterior Biodegradation 57:239–243. https://doi.org/10.1016/j.ibiod.2006.03.001.
8. Keshari N, Adhikary SP. 2014. Diversity of cyanobacteria on stone monuments and building facades of India and their phylogenetic analysis. Int Biodeterior Biodegradation 90:45–51. https://doi.org/10.1016/j.ibiod.2014.01.014.
9. Rossi F, Micheletti E, Bruno L, Adhikary SP, Albertano P, De Philippis R. 2012. Characteristics and role of the exocellular polysaccharides produced by five cyanobacteria isolated from phototrophic biofilms growing on stone monuments. Biofouling 28:215–224. https://doi.org/10.1080/08927014.2012.663751.
10. Albertano P, Urzi C. 1999. Structural interactions among epilithic cyanobacteria and heterotrophic microorganisms in Roman hypogea. Microb Ecol 38:244–252. https://doi.org/10.1007/s002489900174.
11. Ramirez M, Hernandez-Marine M, Novelo E, Roldan M. 2010. Cyanobacteria-containing biofilms from a Mayan monument in Palenque, Mexico. Biofouling 26:399–409. https://doi.org/10.1080/08927011003660404.
12. Hawes I, Howard-Williams C, Vincent WF. 1992. Desiccation and recovery of Antarctic cyanobacterial mats. Polar Biol 12:587–594. https://doi.org/10.1007/BF00236981.
13. Adhikary SP, Sahu JK. 1998. UV protecting pigment of the terrestrial cyanobacterium Tolypothrix byssoidea. J Plant Physiol 153:770–773. https://doi.org/10.1016/S0176-1617(98)80233-2.
14. Douglas S, Beveridge TJ. 1998. Mineral formation by bacteria in natural microbial communities. FEMS Microbiol Ecol 26:79–88. https://doi.org/10.1111/j.1574-6941.1998.tb00494.x.
15. Lisci M, Monte M, Pacini E. 2003. Lichens and higher plants on stone: a review. Int Biodeterior Biodegradation 51:1–17. https://doi.org/10.1016/S0964-8305(02)00071-9.
16. Barabesi C, Galizzi A, Mastromei G, Rossi M, Tamburini E, Perito B. 2007. *Bacillus subtilis* gene cluster involved in calcium carbonate biomineralization. J Bacteriol 189:228–235. https://doi.org/10.1128/JB.01450-06.
17. Stocks-Fischer S, Galinat JK, Bang SS. 1999. Microbiological precipitation of $CaCO_3$. Soil Biol Biochem 31:1563–1571. https://doi.org/10.1016/S0038-0717(99)00082-6.
18. Boquet E, Boronat A, Ramoscor A. 1973. Production of calcite (calcium-carbonate) crystals by soil bacteria is a general phenomenon. Nature 246:527–529. https://doi.org/10.1038/246527a0.
19. Dhami NK, Quirin MEC, Mukherjee A. 2017. Carbonate biomineralization and heavy metal remediation by calcifying fungi isolated from karstic caves. Ecol Eng 103:106–117. https://doi.org/10.1016/j.ecoleng.2017.03.007.
20. Bindschedler S, Cailleau G, Verrecchia E. 2016. Role of fungi in the biomineralization of calcite. Minerals 6:41. https://doi.org/10.3390/min6020041.
21. Burford EP, Hillier S, Gadd GM. 2006. Biomineralization of fungal hyphae with calcite ($CaCO_3$) and calcium oxalate mono- and dihydrate in carboniferous limestone microcosms. Geomicrobiol J 23:599–611. https://doi.org/10.1080/01490450600964375.
22. Lowenstam HA, Weiner S, Jablonski D. 1990. On biomineralization. J Geol 98:977.
23. Mann S. 1995. Biomineralization and biomimetic materials chemistry. J Mater Chem 5:935–946. https://doi.org/10.1039/jm9950500935.
24. Brennan ST, Lowenstein TK, Horita J. 2004. Seawater chemistry and the advent of biocalcification. Geology 32:473–476. https://doi.org/10.1130/G20251.1.
25. Rivadeneyra MA, Delgado R, Delmoral A, Ferrer MR, Ramos-Cormenzana A. 1994. Precipitation of calcium-carbonate by Vibrio spp. from an inland saltern. FEMS Microbiol Ecol 13:197–204. https://doi.org/10.1111/j.1574-6941.1994.tb00066.x.
26. Zamarreño DV, Inkpen R, May E. 2009. Carbonate crystals precipitated by freshwater bacteria and their use as a limestone consolidant. Appl Environ Microbiol 75:5981–5990. https://doi.org/10.1128/AEM.02079-08.
27. Bäuerlein E. 2003. Biomineralization of unicellular organisms: an unusual membrane biochemistry for the production of inorganic nano- and microstructures. Angew Chem Int Ed Engl 42:614–641. https://doi.org/10.1002/anie.200390176.
28. Rivadeneyra MA, Delgado G, Ramos-Cormenzana A, Delgado R. 1998. Biomineralization of carbonates by Halomonas eurihalina in solid and liquid media with different salinities: crystal formation sequence. Res Microbiol 149:277–287. https://doi.org/10.1016/S0923-2508(98)80303-3.
29. Jroundi F, Schiro M, Ruiz-Agudo E, Elert K, Martin-Sanchez I, Gonzalez-Munoz MT, Rodriguez-Navarro C. 2017. Protection and consolidation of stone heritage by self-inoculation with indigenous carbonatogenic bacterial communities. Nat Commun 8:279. https://doi.org/10.1038/s41467-017-00372-3.
30. Giuliani SE, Frank AM, Corgliano DM, Seifert C, Hauser L, Collart FR. 2011. Environment sensing and response mediated by ABC transporters. BMC Genomics 12(Suppl 1):S8. https://doi.org/10.1186/1471-2164-12-S1-S8.
31. Griffin PS, Indictor N, Koestler RJ. 1991. The biodeterioration of stone—a review of deterioration mechanisms, conservation case-histories, and treatment. Int Biodeterior 28:187–207. https://doi.org/10.1016/0265-3036(91)90042-P.
32. Diaz-Herraiz M, Jurado V, Cuezva S, Laiz L, Pallecchi P, Tiano P, Sanchez-Moral S, Saiz-Jimenez C. 2013. The actinobacterial colonization of Etruscan paintings. Sci Rep 3:1440. https://doi.org/10.1038/srep01440.
33. Groth I, Vettermann R, Schuetze B, Schumann P, Saiz-Jimenez C. 1999. Actinomycetes in karstic caves of northern Spain (Altamira and Tito Bustillo). J Microbiol Methods 36:115–122. https://doi.org/10.1016/S0167-7012(99)00016-0.
34. Saizjimenez C. 1995. Microbial melanins in stone monuments. Sci Total Environ 167:273–286. https://doi.org/10.1016/0048-9697(95)04588-R.
35. Keshari N, Adhikary SP. 2013. Characterization of cyanobacteria isolated from biofilms on stone monuments at Santiniketan, India. Biofouling 29:525–536. https://doi.org/10.1080/08927014.2013.794224.
36. Dakal TC, Arora PK. 2012. Evaluation of potential of molecular and physical techniques in studying biodeterioration. Rev Environ Sci Biotechnol 11:71–104. https://doi.org/10.1007/s11157-012-9264-0.
37. Tiano P, Biagiotti L, Mastromei G. 1999. Bacterial bio-mediated calcite precipitation for monumental stones conservation: methods of evaluation. J Microbiol Methods 36:139–145. https://doi.org/10.1016/S0167-7012(99)00019-6.
38. Faust K, Sathirapongsasuti JF, Izard J, Segata N, Gevers D, Raes J, Huttenhower C. 2012. Microbial co-occurrence relationships in the human microbiome. PLoS Comput Biol 8:e1002606. https://doi.org/10.1371/journal.pcbi.1002606.
39. Faust K, Raes J. 2016. CoNet app: inference of biological association networks using Cytoscape. F1000Res 5:1519. https://doi.org/10.12688/f1000research.9050.1.
40. Berry D, Widder S. 2014. Deciphering microbial interactions and detecting keystone species with co-occurrence networks. Front Microbiol 5:219. https://doi.org/10.3389/fmicb.2014.00219.
41. Langille MGI, Zaneveld J, Caporaso JG, McDonald D, Knights D, Reyes JA, Clemente JC, Burkepile DE, Thurber RLV, Knight R, Beiko RG, Huttenhower C. 2013. Predictive functional profiling of microbial communities using 16S rRNA marker gene sequences. Nat Biotechnol 31:814–821. https://doi.org/10.1038/nbt.2676.
42. Feng Q, Liang SS, Jia HJ, Stadlmayr A, Tang LQ, Lan Z, Zhang DY, Xia HH, Xu XY, Jie ZY, Su LL, Li XP, Li X, Li JH, Xiao L, Huber-Schonauer U, Niederseer D, Xu X, Al-Aama JY, Yang HM, Wang J, Kristiansen K, Arumugam M, Tilg H, Datz C, Wang J. 2015. Gut microbiome development along the colorectal adenoma-carcinoma sequence. Nat Commun 6:6528. https://doi.org/10.1038/ncomms7528.
43. Nguyen NH, Song ZW, Bates ST, Branco S, Tedersoo L, Menke J, Schilling JS, Kennedy PG. 2016. FUNGuild: an open annotation tool for parsing fungal community datasets by ecological guild. Fungal Ecol 20:241–248. https://doi.org/10.1016/j.funeco.2015.06.006.
44. Toju H, Kishida O, Katayama N, Takagi K. 2016. Networks depicting the fine-scale co-occurrences of fungi in soil horizons. PLoS One 11:e0165987. https://doi.org/10.1371/journal.pone.0165987.
45. Kubartová A, Ottosson E, Dahlberg A, Stenlid J. 2012. Patterns of fungal communities among and within decaying logs, revealed by 454 sequencing. Mol Ecol 21:4514–4532. https://doi.org/10.1111/j.1365-294X.2012.05723.x.

46. Peay KG. 2014. Back to the future: natural history and the way forward in modern fungal ecology. Fungal Ecol 12:4–9. https://doi.org/10.1016/j.funeco.2014.06.001.
47. Tedersoo L, Bahram M, Polme S, Koljalg U, Yorou NS, Wijesundera R, Ruiz LV, Vasco-Palacios AM, Thu PQ, Suija A, Smith ME, Sharp C, Saluveer E, Saitta A, Rosas M, Riit T, Ratkowsky D, Pritsch K, Poldmaa K, Piepenbring M, Phosri C, Peterson M, Parts K, Partel K, Otsing E, Nouhra E, Njouonkou AL, Nilsson RH, Morgado LN, Mayor J, May TW, Majuakim L, Lodge DJ, Lee SS, Larsson KH, Kohout P, Hosaka K, Hiiesalu I, Henkel TW, Harend H, Guo LD, Greslebin A, Grelet G, Geml J, Gates G, Dunstan W, Dunk C, Drenkhan R, Dearnaley J, De Kesel A, et al. 2014. Global diversity and geography of soil fungi. Science 346:1256688. https://doi.org/10.1126/science.1256688.
48. Lan W, Li H, Wang WD, Katayama Y, Gu JD. 2010. Microbial community analysis of fresh and old microbial biofilms on Bayon temple sandstone of Angkor Thom, Cambodia. Microb Ecol 60:105–115. https://doi.org/10.1007/s00248-010-9707-5.
49. Teske A, Sigalevich P, Cohen Y, Muyzer G. 1996. Molecular identification of bacteria from a coculture by denaturing gradient gel electrophoresis of 16S ribosomal DNA fragments as a tool for isolation in pure cultures. Appl Environ Microbiol 62:4210–4215.
50. White TJ, Bruns T, Lee S, Taylor J. 1990. Amplification and direct sequencing of fungal ribosomal RNA genes for phylogenetics, p 315–322. *In* Innis MA, Gelfand DH, Sninsky JJ, White TJ (ed), PCR protocols: a guide to methods and applications. Academic Press, New York, NY. https://nature.berkeley.edu/brunslab/papers/white1990.pdf.
51. De Muynck W, De Belie N, Verstraete W. 2010. Microbial carbonate precipitation in construction materials: a review. Ecol Eng 36:118–136. https://doi.org/10.1016/j.ecoleng.2009.02.006.
52. Rodriguez-Navarro C, Rodriguez-Gallego M, Ben Chekroun K, Gonzalez-Munoz MT. 2003. Conservation of ornamental stone by *Myxococcus xanthus*-induced carbonate biomineralization. Appl Environ Microbiol 69:2182–2193. https://doi.org/10.1128/AEM.69.4.2182-2193.2003.
53. Tambutte E, Tambutte S, Segonds N, Zoccola D, Venn A, Erez J, Allemand D. 2012. Calcein labelling and electrophysiology: insights on coral tissue permeability and calcification. Proc R Soc B Biol Sci 279:19–27. https://doi.org/10.1098/rspb.2011.0733.
54. Moran AL. 2000. Calcein as a marker in experimental studies newly-hatched gastropods. Mar Biol 137:893–898. https://doi.org/10.1007/s002270000390.
55. Ohno Y, Iguchi A, Shinzato C, Gushi M, Inoue M, Suzuki A, Sakai K, Nakamura T. 2017. Calcification process dynamics in coral primary polyps as observed using a calcein incubation method. Biochem Biophys Rep 9:289–294. https://doi.org/10.1016/j.bbrep.2017.01.006.
56. Wilson CA, Beckman DW, Dean JM. 1987. Calcein as a fluorescent marker of otoliths of larval and juvenile fish. Trans Am Fish Soc 116:668–670. https://doi.org/10.1577/1548-8659(1987)116<668:CAAFMO>2.0.CO;2.